J. Iron Steel Res. Int. (2018) 25:1–8
https://doi.org/10.1007/s42243-017-0005-z

ORIGINAL PAPER

Interfacial reaction between oxide inclusion and steel matrix deoxidized by Si and Mn at 1473 K

Xue-liang Zhang[1,2] · Shu-feng Yang[1,2] · Cheng-song Liu[3] · Jing-she Li[1,2] · Qing Liu[1,2] · Gang Liu[1,2]

Received: 27 December 2016 / Revised: 24 April 2017 / Accepted: 4 May 2017 / Published online: 1 February 2018

Abstract
An improved diffusion couple method was used to simulate the dynamic process of the solid-state reaction at the interface between oxide inclusions and a steel matrix deoxidized by Si and Mn during heat treatment at 1473 K. Experimental results indicated that good contact between the oxide and steel matrix was attained after pre-treatment at 1673 K. In addition, the reaction between the oxide and steel matrix at 1673 K was suppressed, and the effect of this reaction on the diffusion couple experiments at 1473 K was minimized. In the diffusion couple experiments, the diffusion of oxygen from the oxide to the steel matrix resulted in the precipitation of fine oxide particles and a decrease in the Mn content in the steel matrix near the interface after heat treatment at 1473 K. With increasing heat treatment time, the widths of the particle precipitation zone (PPZ) and Mn-depleted zone (MDZ) gradually increased. In addition, the solid-state reaction at the interface between the oxide and steel matrix was intense, and the widths of the PPZ and MDZ increased rapidly during the 0–20 h stage of heat treatment, especially during the 0–5 h stage. The interfacial reaction was retarded, and the rates of width expansion of PPZ and MDZ decreased with increasing heat treatment time.

Keywords Oxide inclusion · Diffusion couple · Heat treatment · Solid-state reaction · Interfacial reaction

1 Introduction

Nonmetallic inclusions are inevitable in steel and greatly affect the quality of steel. Secondary refining is the most common and effective method for controlling the characteristics of nonmetallic inclusions in the process of producing high-quality steel [1–8]. However, the inclusions in solid-state steel often react with the steel matrix during rolling and heat treatment, resulting in compositional changes of the inclusions between the final products and those in molten steel [9–13]. Takano et al. [14] investigated the effect of oxide inclusions on the behavior of grain growth in an austenitic stainless steel (Fe–17%Cr–9%Ni–3%Cu-low C, N alloy) deoxidized by Si and Mn. Their results revealed the presence of mainly $MnO–SiO_2$-type inclusions in the as-cast ingot. After heat treatment at 1523 K for 60 min, the decomposition of $MnO–SiO_2$ led to the transformation of partial $MnO–SiO_2$ inclusions with diameter of approximately 1 μm into fine $MnO–Cr_2O_3$ inclusions with diameter of approximately 0.2 μm. The smaller size of these $MnO–Cr_2O_3$ precipitates effectively suppressed grain growth via the pinning effect. Shibata et al. [15, 16] reported the precise conditions resulting in composition changes of oxide inclusions of stainless steel with different concentrations of Si, Mn, Cr, and Ni during heat treatment, and the mechanism of change for $MnO–SiO_2$ inclusions in a Fe–Cr alloy was clarified by diffusion couple experiments. The experimental results indicated that the $MnO–SiO_2$-type inclusions transformed into $MnO–Cr_2O_3$-type inclusions in stainless steel with low Si content after heat treatment. For high Si content, the composition of the oxide inclusions was still $MnO–SiO_2$ with no change. In addition, the diffusion

✉ Shu-feng Yang
yangshufeng@ustb.edu.cn

✉ Cheng-song Liu
liuchengsong@wust.edu.cn

[1] School of Metallurgical and Ecological Engineering, University of Science and Technology Beijing, Beijing 100083, China

[2] Beijing Key Laboratory of Special Melting and Preparation of High-End Metals, Beijing 100083, China

[3] The State Key Laboratory of Refractories and Metallurgy, Wuhan University of Science and Technology, Wuhan 430081, Hubei, China

couple experiments indicated that the diffusion of Mn, Si, and Cr at the interface between the oxide inclusions and Fe–Cr alloy significantly affected the composition of the oxide inclusions during heat treatment at 1473 K. In addition, Kim et al. [17, 18] investigated the solid-state reaction between Fe–Mn–Si alloy and MnO–SiO_2–FeO oxide during heat treatment at 1473 K. Fine particles and white metal particles with high Fe content formed in the alloy near the interface and bulk oxide, respectively, after heat treatment at 1673 and 1473 K.

The small size of these nonmetallic inclusions makes it difficult to observe and analyze the solid-state reaction between the inclusions and steel matrix during heat treatment using typical experimental methods. Therefore, simulations have been conducted by taking the oxide and iron-based alloys diffusion couples to investigate their solid-state reaction during the actual heat treatment. Liu et al. [19–21] developed a new confocal scanning laser microscope (CSLM) technique for melting oxide to produce a diffusion couple. Using this method, the holding time of the diffusion couple at 1700 and 1673 K was decreased as far as possible. The results revealed the clear suppression of the reaction between the oxide and iron-based alloy at 1700 and 1673 K. The solid-state reaction between Al_2O_3–CaO–FeO oxide and Fe–Al–Ca alloy and that between MnO–SiO_2–FeO oxide and Fe–Mn–Si alloy were thus clarified.

However, Kim et al. [17, 18] and Liu et al. [20, 21] mainly investigated the solid-state reaction between MnO–SiO_2–FeO oxide and Fe–Mn–Si alloy at 1473 K for 10 and 50 h, and the research on the dynamic process of the solid-state reaction between the oxide and iron-based alloy during heat treatment is not sufficient. Therefore, in this study, simulations of the solid-state reaction between oxide inclusions and a steel matrix deoxidized by Si and Mn at 1473 K for 5, 10, 20, 30, 40, and 50 h were conducted using the improved diffusion couple method.

Table 1 Initial compositions of alloy and oxide used for diffusion couple experiments (mass%)

Alloy			Oxide		
Fe	Mn	Si	MnO	SiO_2	FeO
Balance	3.1	0.1	66	31	3

2 Experimental method

The compositions of the Fe–Mn–Si alloy and MnO–SiO_2–FeO oxide used in this study are listed in Table 1. According to the experimental results in Ref. [17], the composition of the alloy and oxide reached equilibrium at 1823 K.

The experimental method was almost the same as that described in Ref. [20]. The Fe–Mn–Si alloy was pre-melted using electrolytic iron, ferromanganese, and silicon in a vacuum induction furnace. Then, the alloy was machined into a cylinder (ϕ 5 mm × 3 mm), and a hole of suitable size was manufactured in the alloy to place the oxide. The oxide with the target composition was obtained by melting the reagents MnO, SiO_2, and FeO powders under an Ar atmosphere in an electrical resistance furnace. The contents of Mn, Si, and Fe were analyzed using an electron probe microanalyzer (EPMA). Pre-melting of the oxide at 1673 K to achieve good contact between the oxide and alloy is necessary. In addition, to avoid intense element diffusion between the oxide and alloy at the interface during pre-treatment, the CSLM technique was used to produce diffusion couples. The Fe–Mn–Si alloy containing the prepared oxide was placed in the CSLM, and pure Ar was introduced after the evacuation of the CSLM chamber to 5×10^{-3} Pa. Then, the temperature was increased from room temperature to 1673 K at a rate of 100 K/min. When the oxide was completely melted, which can be observed in the CSLM during heating, the diffusion couple was immediately cooled by cutting off the power of the CSLM. The cooling rate reached approximately 1000 K/min. After that, the diffusion couple sample, an alloy block with the same composition, and Ti foil were sealed into a quartz tube filled with Ar. Finally, the quartz tube was heated at 1473 K for different time. The specific heat treatment conditions are listed in Table 2. After heat treatment, the quartz tube was quenched by ice water, and the morphology and composition of the alloy and oxide at the interface were examined and analyzed using the EPMA.

3 Results

Figure 1 shows the morphology of the interface between the oxide and alloy of the T0–0 diffusion couple after pre-treatment at 1673 K. Good contact between the oxide and alloy was achieved. In addition, some fine particles were also observed in the alloy near the interface. Compared with the results in Ref. [17], the range of the particle precipitated was smaller, indicating that the diffusion of elements at the interface between the oxide and alloy was suppressed during the pre-treatment at

Table 2 Experimental heat treatment conditions at 1473 K

Diffusion couple	T0–0	T0–5	T0–10	T0–20	T0–30	T0–40	T0–50
Heat treatment time/h	0	5	10	20	30	40	50

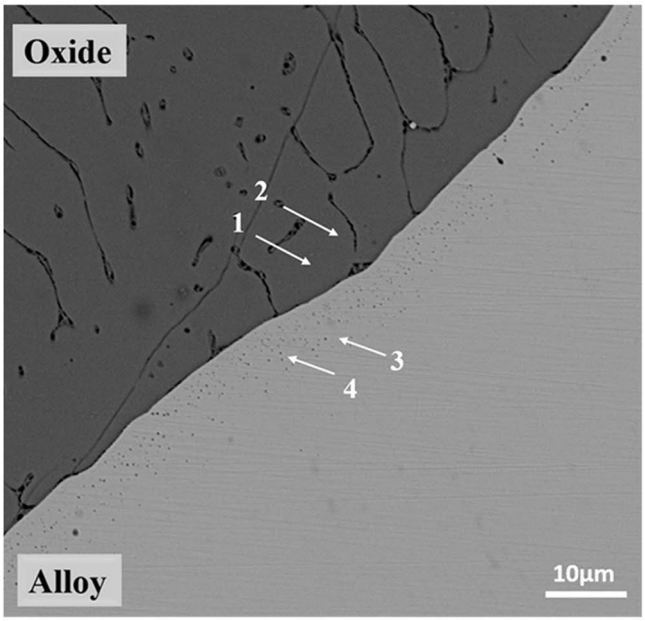

Phase	Position	MnO	SiO_2	FeO
		Mass%		
Slag	1	65.3	31.4	3.3
	2	65.6	31.3	3.1
Particles	3	62.8	37.2	0
	4	60.4	39.6	0

Fig. 1 Morphology of interface between oxide and alloy in T0–0

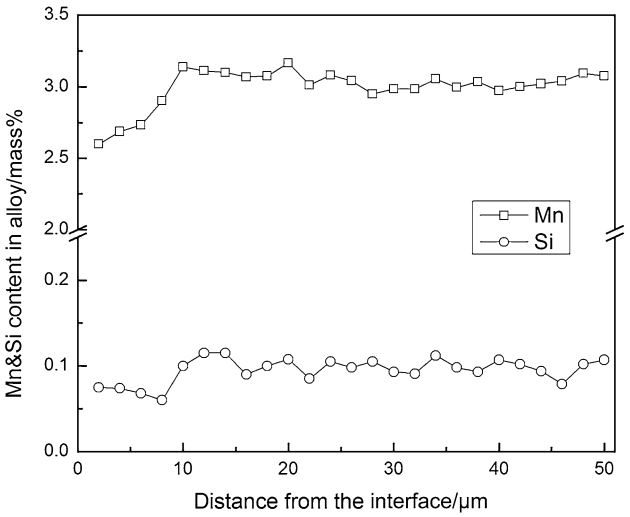

Fig. 2 Change in Mn and Si content in alloy near interface of T0–0

1673 K. In Fig. 1, the oxide was mostly a uniform $2MnO{\cdot}SiO_2$ phase; some black striped patterns were also observed, which were caused by the phase separation during the cooling process in the CSLM. The changes in the Mn and Si contents in the alloy near the interface in the T0–0 diffusion couple are shown in Fig. 2. The Mn and Si contents only decreased slightly in the range of 0–10 μm from the interface from 3.1 to 2.6 mass% and 0.1 to 0.07 mass%, respectively, demonstrating the effective control of elemental diffusion at the interface.

In this study, the method described in Ref. [17] was used to measure the widths of the particle precipitation zone (PPZ) and Mn-depleted zone (MDZ). The widths of the PPZ and MDZ were 6 and 10 μm, respectively.

Figure 3 shows the morphologies of the interface between the oxide and alloy of the diffusion couple T0 after heat treatment at 1473 K for 5–50 h. In addition, the chemical compositions of the oxide near the interface in the diffusion couple T0 after heat treatment are listed in Table 3. After heat treatment at 1473 K for different time, the oxide separated into two phases, a gray phase ($2MnO{\cdot}SiO_2$) and a dark phase ($MnO{\cdot}SiO_2$), and with increasing heat treatment time, the proportion of the dark phase in the oxide increased. In addition, white metal particles with high Fe content were observed in the oxide after heat treatment, which were mainly distributed within $MnO{\cdot}SiO_2$. The size of the metal particles increased with increasing heat treatment time. For the alloy, numerous fine oxide particles formed near the interface after heat treatment at 1473 K for 5 h, as observed in Fig. 3a. With increasing heat treatment time, the width of the PPZ increased, and the number density of precipitated particles decreased; however, the particle size increased.

The changes in the Mn and Si contents in the alloy near the interface are shown in Fig. 4. The minimum value of Mn content gradually decreased upon approaching the interface during the 0–20 h heat treatment stage from 3.1 mass% to approximately 1.4 and 1.1 mass% after heat treatment for 5 and 20 h, respectively. In contrast, after heat treatment for 50 h, the minimum Mn content increased to approximately 2.1 mass% upon approaching the interface. In addition, as observed in Fig. 4, the Mn content slightly increased in the range of 0–30 μm from the interface and increased

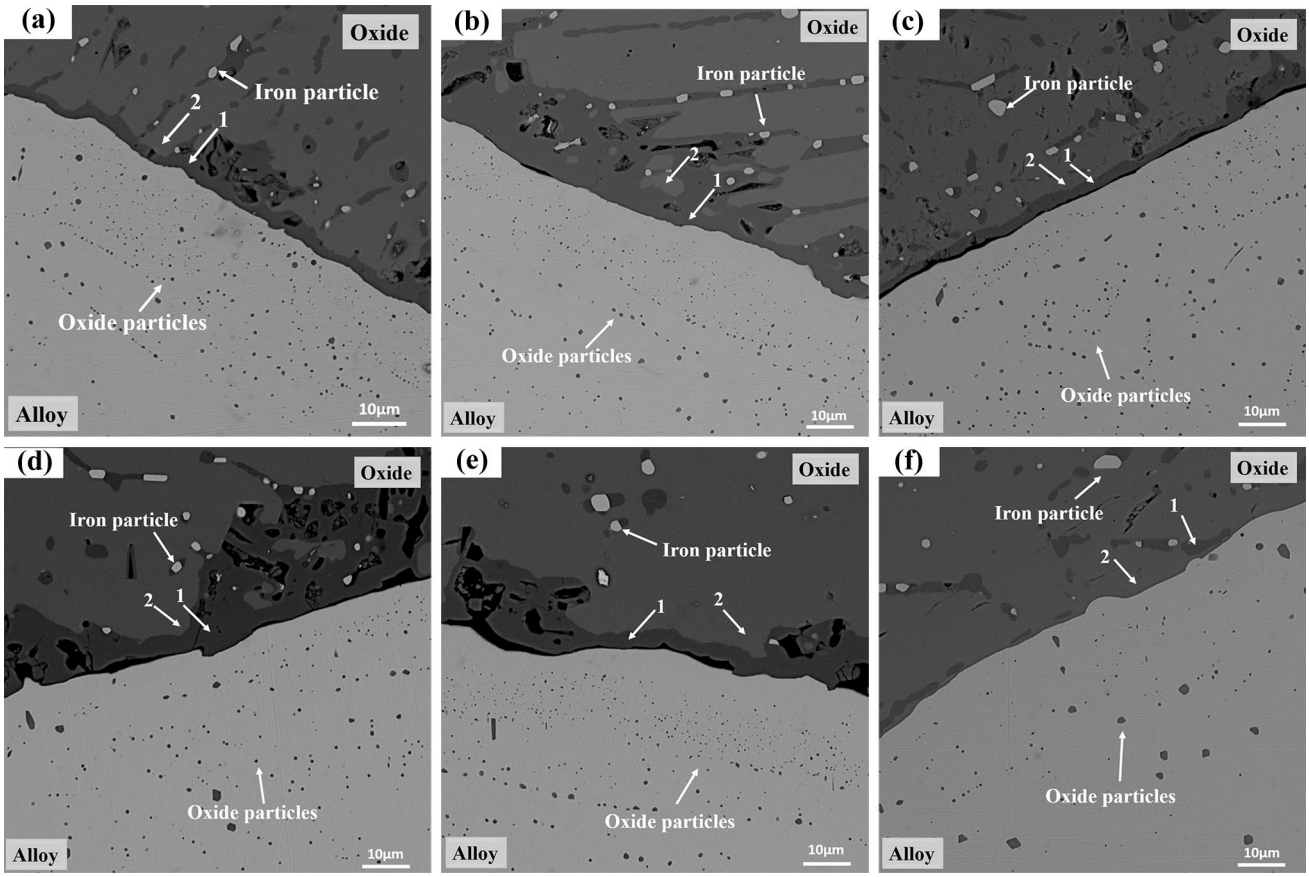

Fig. 3 Morphologies of interface between oxide and alloy of T0 after heat treatment for different time at 1473 K. **a** 5 h; **b** 10 h; **c** 20 h; **d** 30 h; **e** 40 h; **f** 50 h

Table 3 Chemical composition near interface of oxide in diffusion couple T0 after heat treatment for different time

Diffusion couple	Position 1/mass%			Position 2/mass%		
	MnO	SiO_2	FeO	MnO	SiO_2	FeO
T0–5	51.5	46.9	1.6	65.5	32.2	2.3
T0–10	50.4	48.1	1.4	66.1	32.6	1.3
T0–20	51.0	47.2	1.8	66.7	31.7	1.6
T0–30	50.8	48.2	1.0	66.8	32.1	1.1
T0–40	52.5	46.5	1.1	66.4	32.5	1.1
T0–50	54.1	44.6	1.2	65.3	33.6	1.1

continuously with increasing heat treatment time from 1.8 mass% after 5 h to approximately 3.0 mass% after 50 h. With increasing heat treatment time, the width of the MDZ increased. The Si content in the alloy followed similar trends as the Mn content.

Figure 5 reveals that the widths of the MDZ and PPZ increased with heat treatment time at 1473 K, with the width of the MDZ always being larger than that of the PPZ. In addition, the width of the PPZ increased rapidly after heating for 5 h; the growth rate then decreased with increasing heating time. For the MDZ, a large growth rate was maintained in the 0–20 h stage. In the 20–50 h stage, however, the growth rate decreased. A comparison of the widths of the MDZ and PPZ is presented in Fig. 6. The difference between the widths of the MDZ and PPZ increased gradually with increasing heating time from 0 to 20 h. In addition, the difference between the widths of the MDZ and PPZ remained almost constant from 20 to 50 h. A possible explanation for this phenomenon is that the FeO content in the oxide was high and the FeO decomposed rapidly in the early stage

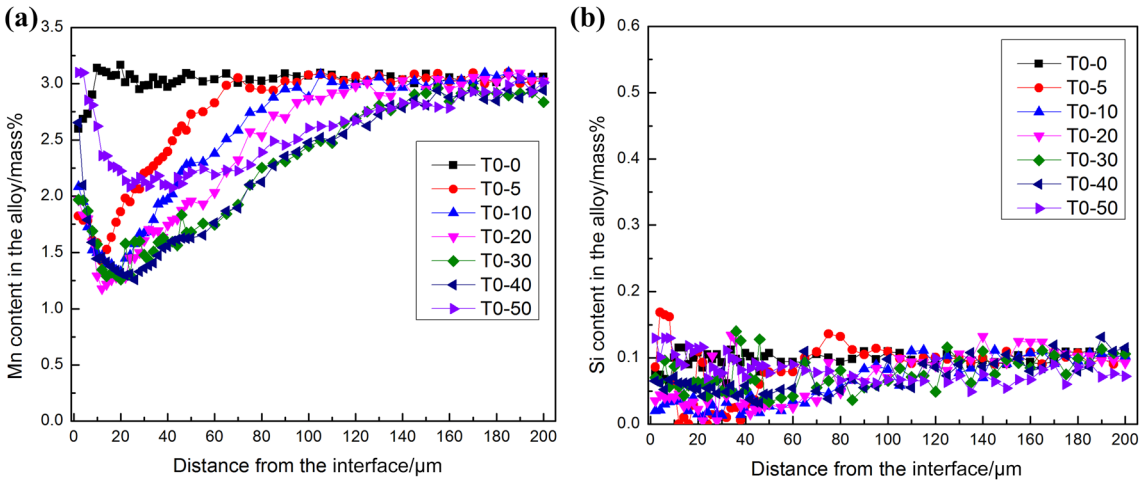

Fig. 4 Change in Mn (**a**) and Si (**b**) contents in alloy near interface

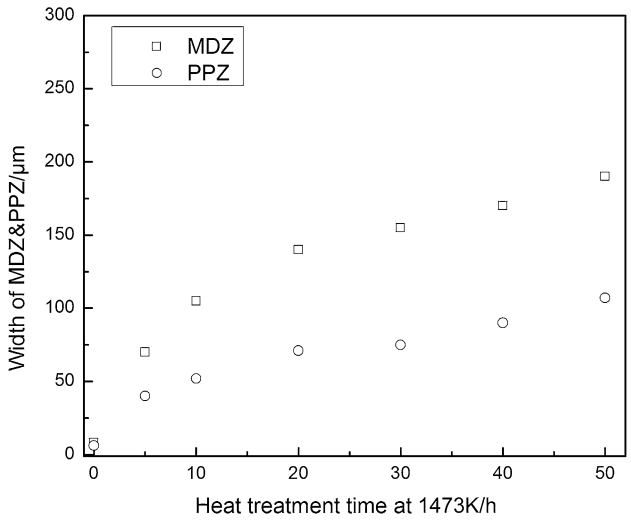

Fig. 5 Change in widths of MDZ and PPZ with heat treatment time at 1473 K

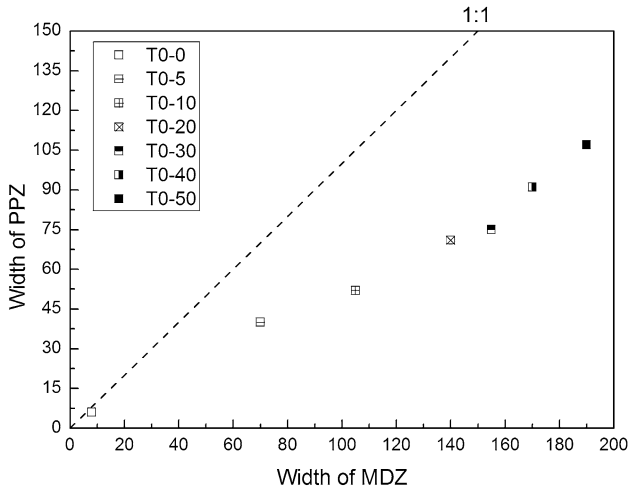

Fig. 6 Comparison of widths of MDZ and PPZ

of the heat treatment, resulting in the rate of oxygen diffusion into the alloy greater than that of the precipitation and growth of the particles in the alloy. With increasing heat treatment time, the FeO content in the oxide decreased, and the rate of oxygen diffusion into the alloy was retarded to a similar level as that of the particle precipitation and growth.

The size distribution of the oxide particles precipitated in the PPZ of the alloy before and after heat treatment at 1473 K is shown in Fig. 7. The method determining the counted area of precipitated oxide particles was the same as that described in Ref. [17]. The width of the counted area was equal to that of the PPZ, and the length of the counted area was 44 μm in the direction parallel to the interface. Most of the oxide particles were small, with diameters of less than 1 μm before heat treatment at 1473 K. Compared

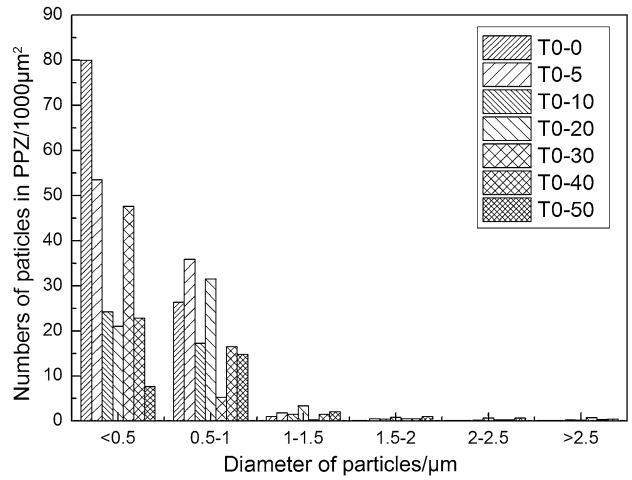

Fig. 7 Size distribution of particles in PPZ before and after heat treatment

with T0–0, the number of particles larger than 1 μm increased after heat treatment at 1473 K. Figure 8 shows the total volume of precipitated particles in the 1000 μm^2 of the PPZ. The precipitated particles were assumed to be spherical to calculate the volume. The results indicate that the total volume of precipitated particles generally increased with increasing heat treatment time, and the total volume of particles clearly increased after heat treatment for 5 h.

4 Discussion

The decomposition of FeO in the oxide and resulting diffusion of excess oxygen from the oxide to the alloy are the main reason for the precipitation of fine particles in the alloy near the interface during the heat treatment, and this phenomenon is similar to internal oxidation [17]. The experimental oxygen partial pressure (P_{O_2}) equilibrated with the oxide at 1473 K was calculated by Eq. (1) [22]. The activity of FeO was calculated by the regular solution model, assuming that the regular solution parameters given in Ref. [23] for liquid oxide were employed to describe the behavior at 1473 K in this study [20].

$$\begin{aligned} &\mathrm{Fe(s)} + 1/2\mathrm{O_2} = \mathrm{(FeO)(s)} \\ &\Delta G^{\theta} = -264430 + 64.73T \end{aligned} \tag{1}$$

The oxidation reactions that may occur in Fe–3.1%Mn–0.1%Si solid solution alloy during heat treatment at 1473 K are shown in Eqs. (2) and (3) [22, 24]. The minimum oxygen pressures under which the Mn and Si in the alloy began to be oxidized are defined as the critical oxygen pressures. The critical oxygen pressures of the Mn ($P_{O_2}^{Mn}$) and Si ($P_{O_2}^{Si}$) were determined by Eqs. (2) and (3), respectively, where the activity coefficients of Mn and Si were assumed to be unity.

$$\begin{aligned} &2[\mathrm{Mn}]_{\mathrm{Fe}} + \mathrm{O_2(g)} = 2\mathrm{MnO(s)} \\ &\Delta G^{\theta} = -809267 + 249.34T \end{aligned} \tag{2}$$

$$\begin{aligned} &[\mathrm{Si}]_{\mathrm{Fe}} + \mathrm{O_2(g)} = \mathrm{SiO_2(s)} \\ &\Delta G^{\theta} = -811537 + 212.55T \end{aligned} \tag{3}$$

The calculated results of the $P_{O_2}^{Mn}$, $P_{O_2}^{Si}$, and P_{O_2} were 2.20×10^{-17}, 2.09×10^{-17}, and 3.20×10^{-15}, respectively. It is found that the experimental oxygen partial pressure was greater than the critical ones of the Mn and Si at 1473 K ($P_{O_2} > P_{O_2}^{Mn} > P_{O_2}^{Si}$), and the Mn and Si elements in the alloy would be oxidized during heat treatment at 1473 K, forming fine oxide particles in the alloy near the interface.

In this study, the dynamic process of the solid-state reaction between the oxide and alloy at the interface during heat treatment at 1473 K was analyzed using the Wagner equation [25]:

$$\xi = \left[\frac{2N_{\mathrm{O}}^{(\mathrm{s})} D_{\mathrm{O}}}{\nu N_{\mathrm{B}}^{(\mathrm{O})}} t\right]^{1/2}, \tag{4}$$

where ξ represents the depth of the internal oxidation zone; $N_{\mathrm{O}}^{(\mathrm{s})}$ is the mole fraction of oxygen at the interface; D_{O} is the diffusivity of oxygen in the alloy; ν is the number of oxygen atoms per A atom in the AO_x oxide; $N_{\mathrm{B}}^{(\mathrm{O})}$ is the mole fraction of the solute element in the alloy; and t is time.

As described in Ref. [20], $N_{\mathrm{O}}^{(\mathrm{s})}$ was determined by the equilibrium relation between the oxide and alloy according to Eq. (1) [22] and Eq. (5) [26]. In the calculation of Eq. (5), the activity coefficient of oxygen was assumed to be unity.

$$\begin{aligned} &1/2\mathrm{O_2}(g) = [\mathrm{O}]\ \text{(in FCC iron)} \\ &\Delta G^{\theta} = -175142 + 60.50T \end{aligned} \tag{5}$$

The diffusivities of oxygen in γ-iron at different temperatures were determined using Eq. (6) [26]. ν was calculated by assuming the formation of $2MnO{\cdot}SiO_2$, and $N_{\mathrm{B}}^{(\mathrm{O})}$ was calculated from the composition of the alloy in this experiment.

$$\log D_{\mathrm{O}} = -\frac{8820}{T} + 0.76 \tag{6}$$

Figure 9 demonstrates the good agreement of the experimental results of the width of the PPZ with the theoretical calculations. As observed in Fig. 4, although some Mn and Si in the oxide also diffused into the alloy during the heat treatment, the effect of this diffusion on the formation of the PPZ and MDZ can be neglected compared with the effect of oxygen at 1473 K.

In addition, as observed in Fig. 9, the dynamic process of the solid-state reaction between the oxide inclusions

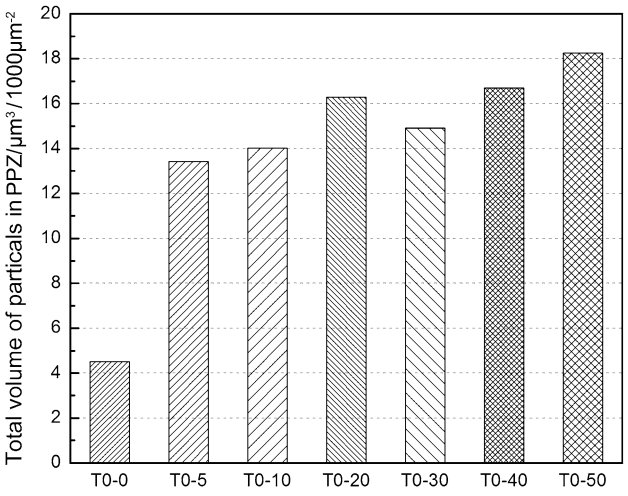

Fig. 8 Total volume of particles in 1000 μm^2 of PPZ

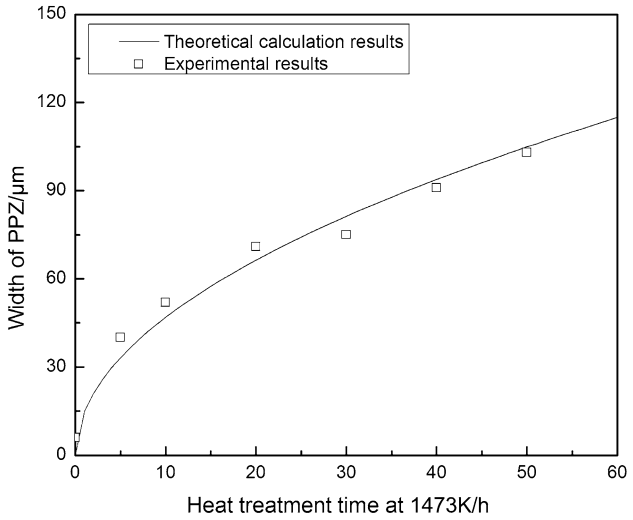

Fig. 9 Comparison of widths of PPZ with theoretical calculations

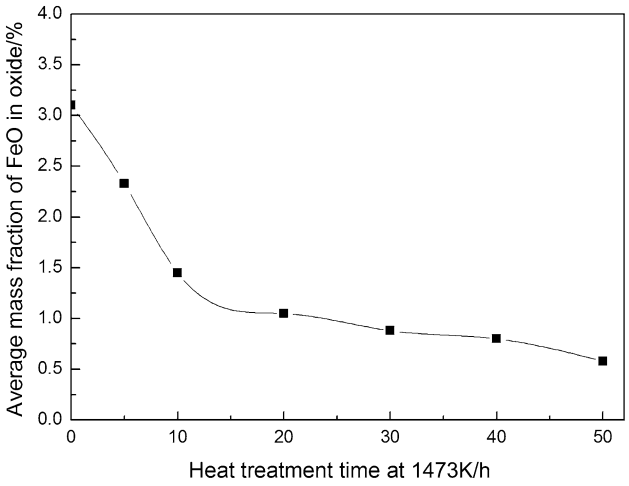

Fig. 10 Change of FeO content in oxide with heating time

and steel deoxidized by Si and Mn during heat treatment at 1473 K was well reflected by the diffusion couple simulations. In the 0–20 h stage of heat treatment, the rates of increase in the widths of the PPZ and MDZ were larger. Especially in the 0–5 h stage, the widths of the PPZ and MDZ increased rapidly from 6 to 40 μm and 8 to 70 μm, respectively. However, in the 20–50 h stage of heat treatment, the rates of increase in the widths of the PPZ and MDZ decreased, only increasing from 71 to 107 μm and 144 to 190 μm after heating for 20 and 50 h, respectively. To clarify the reason for this phenomenon, the oxide components at 20–30 points within 50 μm from the interface were analyzed by the EPMA in this study, and the average value was used as the oxide component at the interface. The change in the FeO content in the oxide at the interface with increasing heating time is depicted in Fig. 10. The FeO content clearly decreased during heat treatment for 0–20 h. In addition, with increasing heating time, the decomposition of FeO became slower. The FeO in the oxide was the source of free oxygen. When a larger amount of FeO was decomposed during heat treatment, the driving force for diffusion of oxygen from the oxide to the alloy was large, and the solid-state reaction between the oxide and alloy at the interface was intense. In contrast, when the FeO decomposed slowly, the solid-state reaction was gentle, which is consistent with the changes in the widths of the PPZ and MDZ.

In addition, as demonstrated in Fig. 4, the Mn and Si contents in the alloy near the interface showed a trend of first decreasing and then increasing, but the contents were still lower than the initial contents. The diffusion coefficient of oxygen in austenite is on the order of 10^{-11} m^2/s, and that of Mn and Si in austenite is on the order of 10^{-13} m^2/s [18]. These values indicate that the diffusion of cations is much slower than that of anions. Therefore, the Mn and Si contents were controlled by the diffusion of oxygen when the heat treatment time was short. With increasing heating time, the effect of the diffusion of Mn and Si from the oxide to the alloy was gradually manifested. In addition, as demonstrated in Figs. 5 and 6, the width of the MDZ was always larger than that of the PPZ after heat treatment for different time at 1473 K. Possible reasons for this finding may be that some precipitated particles were too small to be observed or that the particles underwent coarsening during heat treatment [17]. Furthermore, because of the presence of a concentration gradient of Mn in the alloy near the interface, the diffusion of Mn from the alloy interior to the interface also exacerbated this phenomenon.

5 Conclusions

1. The dynamic process of the solid-state reaction between oxide inclusions and steel deoxidized by Si and Mn during heat treatment at 1473 K was well reflected using the simulation research employing diffusion couples.
2. After heat treatment at 1473 K, the excess oxygen generated from the decomposition of FeO in the oxide diffused into the alloy and reacted with the Mn and Si, resulting in the reduction in Mn and Si contents and precipitation of fine oxide particles in the alloy.
3. The widths of the MDZ and PPZ increased with increasing heat treatment time at 1473 K. In addition, in the 0–20 h stage of heat treatment, especially in the 0–5 h range, the widths of the MDZ and PPZ increased rapidly because of the large decomposition of FeO in the oxide. Upon extending the heat treatment time to 30–50 h, the solid-state reaction between the oxide and alloy at the interface was retarded, and the rates of increasing width of the MDZ and PPZ gradually decreased.

4. A dynamic model for calculating the width of the PPZ near the interface between inclusions and steel deoxidized by Si and Mn during heat treatment at 1473 K was established based on the Wagner equation, and the experimental results for the width of the PPZ agreed well with the theoretical calculations.

Acknowledgements The authors are grateful to the financial support from the National Natural Science Foundation of China (Nos. 51574020, 51674023, and 51604201).

References

[1] F.M. Yuan, X.H. Wang, X.F. Yang, J. Univ. Sci. Technol. Beijing 13 (2006) 486–489.
[2] H. Ono, K. Nakajima, T. Ibuta, T. Usui, ISIJ Int. 50 (2010) 1955–1958.
[3] S.F. Yang, J.S. Li, Z.F. Wang, J. Li, L. Lin, Int. J. Miner. Metall. Mater. 18 (2011) 18–23.
[4] J. Yang, X.H. Wang, M. Jiang, W. J. Wang, J. Iron Steel Res. Int. 18 (2011) No. 7, 8–14.
[5] Z.J. Cheng, J. Guo, S.S. Cheng, J. Iron Steel Res. Int. 20 (2013) No. 2, 14–20.
[6] S.F. Yang, J.S. Li, L.F. Zhang, P. Kent, Z.F. Wang, J. Iron Steel Res. Int. 17 (2010) No. 7, 1–6.
[7] H.X. Yu, X.H. Wang, J. Zhang, W.J. Wang, J. Iron Steel Res. Int. 22 (2015) 573–581.
[8] F. Zhang, G.Q. Li, J. Iron Steel Res. Int. 20 (2013) No. 4, 20–25.
[9] I. Takahashi, T. Sakae and T. Yoshida, Tetsu-to-Hagane 53 (1967) 350–353.
[10] I. Takahashi, T. Sakae, T. Yoshida, Tetsu-to-Hagane 53 (1967) S273.
[11] W.J. Choi, H. Matsuura, F. Tsukihashi, ISIJ Int. 51 (2011) 1951–1956.
[12] J.H. Park, D.S. Kim, Metall. Trans. B 36 (2005) 495–502.
[13] C. Lee, S. Nambu, J. Inoue, T. Koseki, ISIJ Int. 51 (2011) 2036–2041.
[14] K. Takano, R. Nakao, S. Fukumoto, T. Tsuchiyama, S. Takaki, Tetsu-to-Hagane 89 (2003) 616–622.
[15] H. Shibata, K. Kimura, T. Tanaka, S.Y. Kitamura, ISIJ Int. 51 (2011) 1944–1950.
[16] H. Shibata, T. Tanaka, K. Kimura, S.Y. Kitamura, Ironmak. Steelmak. 37 (2010) 522–528.
[17] K.H. Kim, S.J. Kim, H. Shibata, S.Y. Kitamura, ISIJ Int. 54 (2014) 2144–2153.
[18] K.H. Kim, H. Shibata, S.Y. Kitamura, ISIJ Int. 54 (2014) 2678–2686.
[19] C.S. Liu, S.F. Yang, J.S. Li, H.W. Ni, X.L. Zhang, Metall. Trans. B 48 (2017) 1348–1357.
[20] C.S. Liu, K.H. Kim, S.J. Kim, J.S. Li, S. Ueda, X. Gao, H. Shibata, S.Y. Kitamura, Metall. Trans. B 46 (2015) 1875–1884.
[21] C.S. Liu, S.F. Yang, K. Kim, J.S. Li, H. Shibata, S.Y. Kitamura, Int. J. Miner. Metall. Mater. 22 (2015) 811–819.
[22] S. Ban-Ya, E. Tasuhiko, Physical Chemistry of Metals, Maruzen Press, Tokyo, 1996.
[23] S. Ban-Ya, ISIJ Int. 33 (1993) 2–11.
[24] M. Hino, K. Ito, Thermodynamic Data for Steelmaking, Tohoku University Press, Sendai, 2010.
[25] C. Wagner, Z. Elektrochem. 63 (1959) 772–782.
[26] J.H. Swisher, E.T. Turkdogan, Trans. Met. Soc. AIME 239 (1967) 426–431.